J Therm Anal Calorim (2012) 107:555–560
DOI 10.1007/s10973-011-1687-2

Effect of mercaptopropionic acid as linker on structural, thermal, and optical properties of TiO_2–CdSe nanocomposites

S. K. Arya · Tanvi Vats · Shailesh N. Sharma · Kulvir Singh · A. K. Narula

Received: 7 February 2011 / Accepted: 19 May 2011 / Published online: 3 June 2011

Abstract In this study, we have studied the stability of TiO_2–CdSe nanocomposites in which the individual moieties are linked using a bifunctional linker (mercaptopropionic acid). Nanoparticles of TiO_2 and CdSe are synthesized by sol–gel and one pot methods. The equimolar amount of the above particles is utilized to prepare nanocomposites with and without linker. These samples are characterized for their structural, thermal, and optical properties using X-ray diffraction (XRD), differential thermal analysis (DTA), thermogravimetric analysis (TG), Fourier transform infra-red spectroscopy (FTIR), and UV–Vis spectroscopy. The average particle size of TiO_2 and CdSe are 16 and 23 nm, respectively. The addition of a bifunctional linker shows remarkable effect on the properties of TiO_2–CdSe nanocomposites.

Keywords Bifunctional linker · Structural, thermal, and optical stability

Introduction

A lot of efforts have been made by the researchers all over the world to improve the different properties of TiO_2-based materials especially in crystalline TiO_2 nanoparticles (NPs). Remarkable progress has been made in their preparation and applications for photovoltaics, sensors, and photochromic devices [1–3]. The above-mentioned properties of TiO_2 nanoparticles depend on different factors such as size, morphology, crystallinity, phase purity, and solubility (dispersibility) in different host matrices [4–6].

Structurally, titania exists in three polymorphs: brookite, anatase, and rutile. As a bulk material, rutile is stable phase, and thermodynamically metastable anatase phase is usually transformed into rutile phase in the temperature from 600 to 700 °C. So, synthesis of anatase TiO_2 nanocrystals with better quality including thermal stability is always an important parameter [7–10]. In fact, anatase nanocrystals are commonly observed for particle sizes below 15 nm [11], although higher crystal sizes, from 15 to 50 nm [12], have also been reported in the literature. This fact is explained by the dependance of anatase stabilization of several parameters, such as pH media, synthesis temperature, and moreover surface energy of anatase is lower than those of rutile and brookite [13].

Consequently, structure and particle size are the two most important parameters that influence physical properties of TiO_2. In addition, the transformation may also be affected by preparation conditions, precursors, impurities, and oxygen vacancies and so on. Although, TiO_2 is very stable photoelectrode and has good corrosion resistance in aqueous solution, due to its high energy band gap (3.2 eV), efficient absorption of visible light is prevented leading to poor conversion efficiency. The electronic conversion efficiency can be enhanced on doping lower-band gap materials such as narrow-band gap semiconductor materials like CdSe [14–16]. Furthermore, a favorable link is also required between CdSe and TiO_2 nanoparticles for efficient transfers of electron injection [17]. Therefore, to improve

S. K. Arya · K. Singh
School of Physics and Material Science, Thapar University, Patiala 147001, India

T. Vats · A. K. Narula
University School of Basic and Applied Sciences, Guru Gobind Singh Indraprastha University, Delhi 110403, India

S. N. Sharma (✉)
Physics of Energy Harvesting Division, National Physical Laboratory, Dr. K.S. Krishnan Marg, New Delhi 110012, India
e-mail: shailesh@mail.nplindia.ernet.in

the coupling between CdSe and TiO_2, bifunctional linker like mercaptopropionic acid (MPA) is required [18]. It has both thiol and carboxylic group which, respectively, bind with CdSe and TiO_2, in turn linking both the nanoparticles [19–21]. An efficient coverage of quantum dots on titania nanoparticles is a prerequisite for charge transfer. So, it is important to study the effect of CdSe and linker on various properties of TiO_2 nanoparticles. In the present study, TiO_2 and 0.5:1 CdSe nanoparticles are synthesized by chemical method. The nanocomposites of the two nanoparticles are prepared with and without the aid of bifunctional linker (mercaptopropionic acid) and characterized by X-ray diffraction (XRD), Fourier transform infra-red spectroscopy (FTIR), Thermal gravimetric analysis (TGA)/Differential thermal analysis (DTA), and UV–Vis spectroscopic techniques.

Experimental

Synthesis of TiO_2 nanoparticles was carried out using sol–gel method. The materials used were titanium isopropoxide (Sigma–Aldrich, 99.9% purity), Isopropanol(Sigma–Aldrich, 99.9% purity), and glacial acetic acid (Sigma–Aldrich). A solution of titanium isopropoxide in isopropanol was added to water and glacial acetic acid solution placed in an ice bath. The mixture was constantly stirred, and a cloudy white precipitate was observed. The precipitate was then placed in a water bath at 80 °C with constant stirring to obtain a gel-like entity which became milky on cooling down. This colloidal solution obtained was placed in a sealed glass flask and kept in a vacuum oven at 200 °C for 12 h and then cooled to the room temperature to obtain white colloidal TiO_2 solution with a bluish tint. The solution obtained was stable for months and could be used after stirring [22]. The synthesis of CdSe nanoparticles were carried out by the chemical route using TOP/TOPO capping method to arrest the growth of the nanoparticles to desired sizes, the detail of which can be found elsewhere. 0.5:1 refers to the ratio of cadmium precursor (CdO) to that of selenium precursor (TOP Se) [23]. The materials used were of the purest quality available and used as received. Cadmium oxide (CdO; Aldrich, 99.99% purity), tetradecylphosphonic acid (TDPA; Alfa Aesar, 98% purity), trioctylphosphine oxide (TOPO; Aldrich, 99% purity), trioctylphosphine (TOP; Aldrich, 90% purity), and selenium powder (Aldrich, 99.5% purity) were used.The CdSe quantum dots (QDs) either by direct adsorption or with the aid of bi-functional linker molecule (mercaptopropionic acid) [15] were anchored on the surface of the sol–gel-prepared nanoporous TiO_2 layers in tetrahydrofuran (THF)–ethanol (1:1) solvent.

The X-ray diffraction (XRD) studies were done by using a Siemens D500 X-ray Diffractometer (Cu Kα ~1.5406 Å). The UV–Vis absorption spectra were recorded using Shimadzu 3101 spectrometer. FTIR spectra were taken using a Perkin Elmer Bx system. TGA and DTA curves were recorded using a Perkin Elmer Diamond Pyris system.

Results and discussion

XRD analysis

The XRD pattern of TiO_2, CdSe, TiO_2 + CdSe, and TiO_2 + CdSe + linker are shown in Fig. 1a–d.

XRD pattern of TiO_2 nanoparticles exhibit only few peaks. These peaks are indexed with the anatase phase of TiO_2 (JCPDS-21-1272). The strongest peak is observed at (101) plane in TiO_2 nanoparticles. In the case of CdSe, all the XRD peaks are identified as wurtzite phase. When both the nanoparticles are mixed in equimolar amount, they show some broadening in the XRD peaks. Obviously, the mixed phase consists of higher disordering than the pure phase as evident in Fig. 1a–c. A careful observation of both the XRD patterns reveals that the XRD peaks are relatively sharper in CdSe as compared with TiO_2 nanoparticles sample. As observed in from Fig. 1c and d the XRD peaks become broader than the virgin samples of TiO_2 and CdSe. In addition to this, with linker Fig. 1d, the XRD peak at ~25° splits into two peaks. It might be possible that the linker plays an important role in linking CdSe and TiO_2 nanoparticles. In Fig. 1c, the broadening of (100) peak might be a resultant of the overlapping of CdSe(100) and

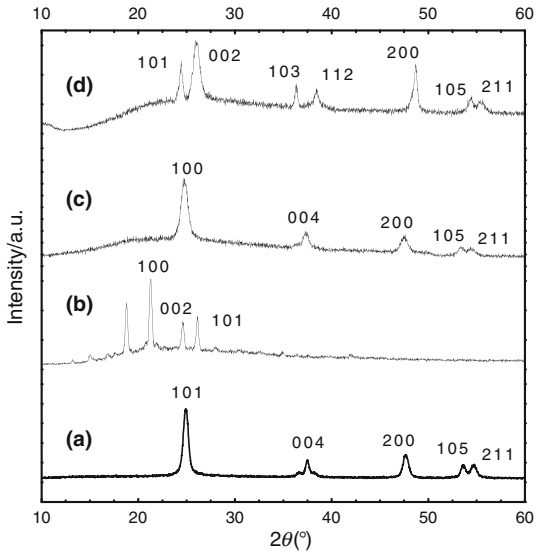

Fig. 1 XRD pattern (*a*) TiO_2, (*b*) CdSe, (*c*) TiO_2 + CdSe, (*d*) TiO_2 + CdSe + linker

TiO_2(101). It is the manifestation of higher particle size CdSe than that of the TiO_2 sample. The confirmation of this hypothesis was done using the Scherrer formula [24]

$$D = K\lambda/\beta \cos\theta \quad (1)$$

where D is the crystal size of the sample, λ is the X-ray wavelength (1.54 Å) of incident radiation, β the full width at half maximum (FWHM) of the diffraction peak in radian, K is a coefficient (0.89), and θ is the diffraction angle at the peak maximum. The calculated average particle sizes are summarized in Table 1. The particle size decreases when CdSe and linker add on TiO_2 nanoparticles. This could be attributed due to the competition among different cations which are present in the samples (c) and (d). After using the Scherrer formula, the average crystallites size of samples (a) and (b) were found to be 16 and 23 nm, respectively. On the other hand, (c) and (d) consist of the particle size ~9 and 10 nm, respectively. It seems that either the linker prevents the agglomeration of nanoparticles or due to disordering effect, the XRD pattern becomes broader, and using these XRD peaks for particle size calculation is not appropriate.

FTIR spectroscopy

To probe the charge transfer across CdSe–TiO_2 composites, FTIR transmittance spectra of pure TiO_2, CdSe nanocrystallites, and their respective composites in the absence and presence of linker (MPA) in THF:ethanol (1:1) solvent were taken (Fig. 2a–d). Spectra of TiO_2 show transmittance band at ~3000 and ~1600 cm^{-1} which can be attributed to the adsorption of H_2O and –OH of TiO_2 [25], respectively. A band at ~2365 cm^{-1} corresponds to C–H bending mode; a band at ~1600 cm^{-1} is assigned to C–C ring stretching modes. The broad bands at ~900 cm^{-1} can be assigned to the Ti–O band in TiO_2. The broad characteristic intense band below 1104 cm^{-1} is due to Ti–O–Ti vibration mode [25]. The FTIR spectrum of pure TiO_2 is greatly modified by the presence of CdSe QDs for both with and without linker samples (Fig. 2a, c, d). For pure CdSe (2:1) (Fig. 2b), the FTIR spectra exhibits well-defined main peaks: ~2980, 2371, and 889 cm^{-1} corresponding to the CH-stretching (sp3), CH-bending, and methylene ($–CH_2$) vibrational modes [26], respectively. However, the presence of IR peak ~1081 cm^{-1} corresponds to P=O stretching vibrational modes [26, 27], thus, indicating the presence of capping agent TOP/TOPO bounded to CdSe nanocrystals, respectively. For TiO_2–CdSe nanocomposites corresponding to with linker (MPA) system, the presence of C–H stretching modes, C–O stretching modes, alkyl wagging, and twisting modes at ~2900–3000, 1550–1620, 1090–1110 cm^{-1} [28], respectively, in the spectra (Fig. 2d) provides clear evidence for the attachment of linker MPA to the TiO_2 surface. The changes in the C–O stretching region of CdSe–TiO_2 nanocomposites spectrum with linker (MPA) (Fig. 2d) as compared with pure TiO_2 spectrum (Fig. 2a) indicate that MPA binds to the TiO_2 surface through the carboxylic acid group. However, such marked changes were not observed in the case of FTIR spectra (Fig. 2c), i.e., for TiO_2–CdSe nanocomposites without linker.

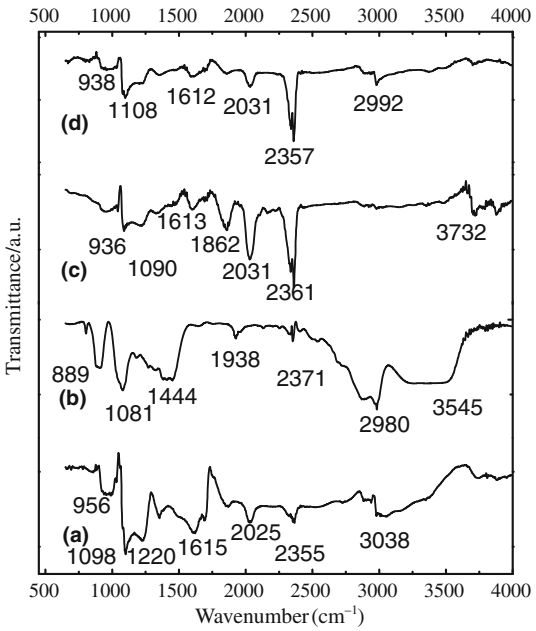

Fig. 2 FTIR spectra (*a*) TiO_2, (*b*) CdSe, (*c*) TiO_2 + CdSe, (*d*) TiO_2 + CdSe + linker

Thermal analysis

In order to understand the thermal stability, samples (a), (b), (c), and (d) were investigated using TG and DTA measurements. The TG curve (Fig. 3) of sample (a) consists of two mass loss regions at 350 and ~800 °C. Similarly, DTA (Fig. 4) curve of the sample exhibit a broad exothermic peak at 350 °C. However, at a higher temperature, DTA curve could not show any endo/exothermic peaks as observed mass loss in TG curve of TiO_2 sample. The total mass loss is 6% up to 350 °C, and in a higher temperature, it is only 1.5% as indicated in TG curve. In the first region, the major mass loss might be ascribed due to the oxidation of organic impurities such as carbon residue since during the preparation of TiO_2 nanoparticles titanium isopropoxide was taken as initial ingredient [29]. A small mass loss (~1.6%) in second region is due to the loss of chemically bound water in sample (a). Moreover, the mass loss is not very appreciable which is again manifestation of this kind of mass loss [30]. On the other hand, a very sharp exothermic peak is observed in DTA curve of sample (b). A sharp mass loss is also observed in TG curve

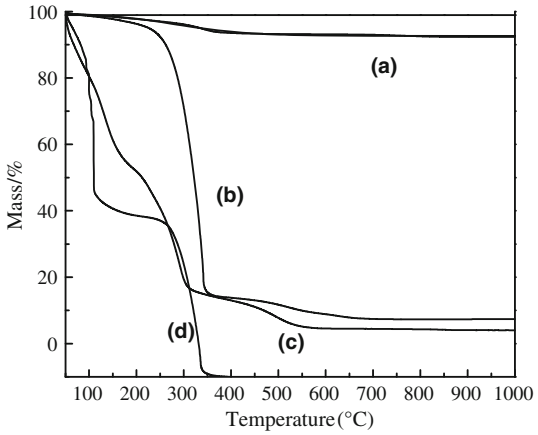

Fig. 3 TG Curves (*a*) TiO_2, (*b*) CdSe, (*c*) TiO_2 + CdSe, (*d*) TiO_2 + CdSe + linker

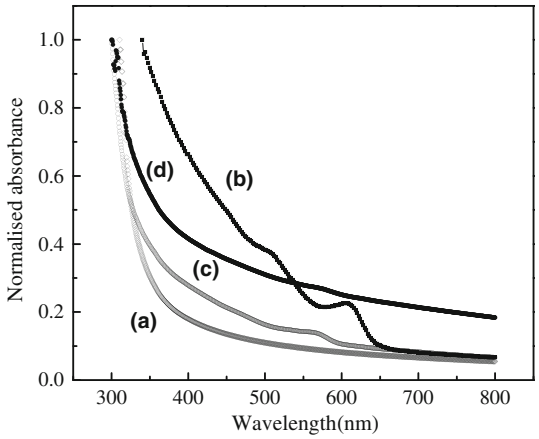

Fig. 5 Absorption spectra (*a*) TiO_2, (*b*) CdSe, (*c*) TiO_2 + CdSe, (*d*) TiO_2 + CdSe + linker

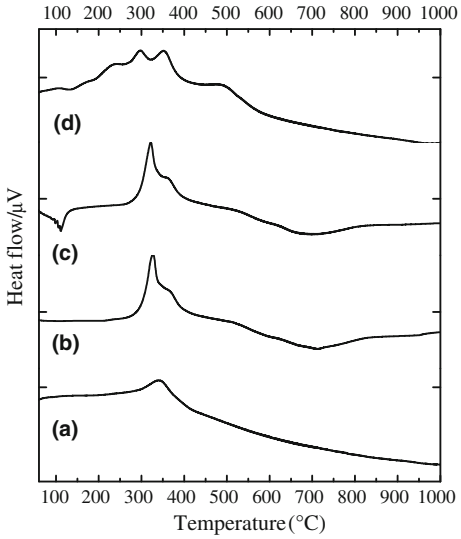

Fig. 4 DTA curves (*a*) TiO_2, (*b*) CdSe, (*c*) TiO_2 + CdSe, (*d*) TiO_2 + CdSe + linker

of the same sample. This corresponds to the disintegration of capping agent of CdSe quantum dots at that temperature. Interestingly, TG/DTA curves of samples (c) and (d) exhibit an endothermic peak at ~110 °C. The presence of this peak became suppressed in the sample (d) where linker was used. This indicates the removal of TOPO capping from CdSe quantum dots by the thiol group of the linker. The endothermic peak could be associated with water evaporation. However, in the case of the sample (d), the OH group from water might be linked with the linker in sample (d), which leads to the less evaporation of water. The exothermic peak in both the samples evolves due to the decomposition of the organic substances. A mass loss of more than 100% is being observed in TG curve of sample (d). It is because Pt crucible was used using Al_2O_3 as reference, and Al_2O_3 might be evaporated along with sample during TG/DTA experiment. The addition of the linker in sample (d) decreases its thermal stability.

UV–Vis spectroscopy

Figure 5 shows the normalized UV–Vis absorption of TiO_2 nanocrystals and TiO_2/CdSe colloidal capped by TOPO (Tri-*n*-octylphosphine oxide) in Toluene with and without linker. The absorbance spectra of various synthesized samples were studied. According to Tauc, a number of materials in their absorbance spectra show three regions of variation of absorption coefficient with the photon energy. The first region that is known as "Tauc region" corresponds to the high absorption from which optical band gap can be calculated [31]. The absorption spectra of TiO_2 consists of a single sharp band around 309 nm. The characteristic absorption is due to the charge-transfer from the valence band (mainly formed by 2p orbitals of the oxide anions) to the conduction band (mainly formed by $3dt_2g$ orbitals of the Ti^{4+} cations) [32]. The more weakly these electrons are bound, the more easily the absorption occurs. For Tauc's region, absorption coefficient is given in more general form:

$$\alpha h\upsilon = A\left(h\upsilon - E_g\right)^n \quad (2)$$

where α is the absorption coefficient, $h\upsilon$ is the photon energy, E_g is the optical band gap, and A is a constant. Here, n is an index that has different value depending upon the mechanism of interband transitions, i.e., 2,3,1/2, and 1/3 values corresponding to indirect allowed, indirect forbidden, direct allowed, and direct forbidden. $\sqrt{\alpha h\upsilon}$ was plotted as a function of $h\upsilon$, and the linear region was extrapolated to zero absorption to estimate E_g. A good fit observed between Eq. 1 and experimental data indicates that nanoparticles exhibit a indirect band gap and are listed

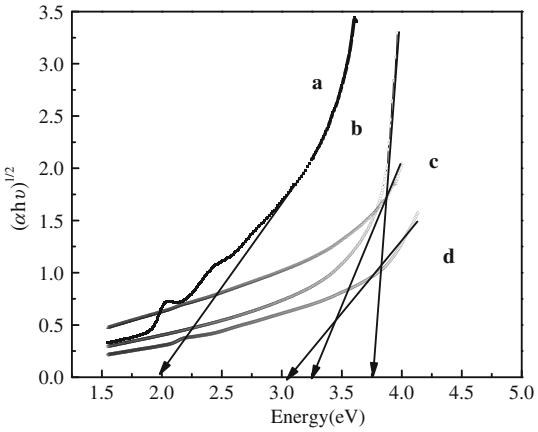

Fig. 6 Tauc's plots (*a*) TiO_2, (*b*) CdSe, (*c*) TiO_2 + CdSe, (*d*) TiO_2 + CdSe + linker

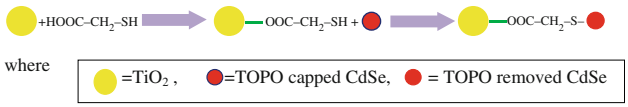

Fig. 7 Pictorial representation of the role of linker in anchoring CdSe on TiO_2 nanoparticles

in Table 1. Both the direct and indirect band gap can be found as well in anatase structure [33]. In the case of anatase, there is a consensus that the absorption edge is around 3.2 eV, associated with indirect transitions [34, 35]. The optical anisotropy and the controversy about the existence of size quantization effects introduce additional complexity in the analysis of optical response of anatase nanoparticles [36] (Fig. 6).

Another interesting feature to be noted is, in the beginning, the absorption is quite sharp (curves (a)–(c)); later it exhibits a broad hump. This is quite similar to the Urbach edge that is generally observed both in crystalline and non-crystalline semiconductors [37]. This second region known as "Urbach region" is an exponential region due to the structural disorientation and randomness of the system. In crystalline materials, it is believed to be due to band tailing associated with disorder produced by thermal fluctuations in crystal lattice. For small absorption coefficients, there is usually an Urbach tail where $\alpha(\upsilon)$ depends exponentially on the photon energy $h\upsilon$ as follows [38]:

$$\alpha(\upsilon) = \alpha_0 \exp(h\upsilon/E_u) \quad (3)$$

where α_0 is the constant and E_u is Urbach energy which is the width of the tails of localized states in the band gap representing degree of disorder. E_u Values are calculated from slopes of linear portion of the curve between ln (α) against $h\upsilon$.

On the basis of above discussions, the role of mercaptopropionic acid as linker can be elucidated by the pictorial representation as depicted in Fig. 7.

Conclusions

From the above studies, the role of bifunctional linker in effective attachment of CdSe quantum dots on the TiO_2 was detected. Mercaptopropionic acid is a bifunctional compound with a carboxylic group (–COOH) at one end and a thiol group (–SH) at the other. The thiol group attaches itself to CdSe while the carboxylic group links itself to TiO_2. From the TGA curve, it is very clear that the capping agent has been removed by the thiol group of the linker. The analysis of XRD peaks also gives an insight into the interparticle role of the linker indicating the adhesion of titania nanoparticles with CdSe quantum dots. Removal of the capping agent and proper adhesion of quantum dots on the semi conductor oxides play a vital role in the photovoltaic and photocatalytic application of the above hybrids. The capping agent on semiconductor quantum dots play a vital role in the size confinement and surface passivation of the quantum dots during the synthesis. However, when we use quantum dots as a sensitizer for photovoltaic or photocatalytic applications using an appropriate linker MPA, the thiol end of it replaces the TOP/TOPO capping from CdSe QD's while its other end consisting of carboxylic acid "COOH" group is attached to TiO_2, thus, the linker acts as a bridge and an effective contact between the two components CdSe and TiO_2 nanocrystals which in turn results in efficient charge transfer between the quantum dot and the semiconductor oxide.

Table 1 A comparative study of the effect of linker on the properties of TiO_2-quantum dot nanohybrids

Sample	Critical absorption wavelength/nm	Optical band gap, E_g/eV	Urbach energy, E_u/eV	Particle size by XRD/nm
(a) TiO_2	309	3.79	0.53	16
(b) CdSe	339	2.0	0.086	23
(c) TiO_2 + CdSe	306	3.5	0.56	9.3
(d) TiO_2 + CdSe + linker	300	3.1	1.26	10

References

1. Fisher AC, Peter LM, Ponomarev EA, Walker AB, Wijayantha KGU. Intensity dependence of the back reaction and transport of electrons in dye-sensitized nanocrystalline TiO_2 solar cells. J Phys Chem B. 2000;4:949–58.
2. Biancardo M, Argazzi R, Bignozzi CA. Solid-state photochromic device based on nanocrystalline TiO_2 functionalized with electron donor–acceptor species. Inorg Chem. 2005;44:9619–21.
3. Yang T, Lin H, Wei B, Wu C, Lin C. Enhancement of the gas sensing properties of nano-TiO_2. Rev Adv Mater Sci. 2003;4: 48–54.
4. Wold A. Photocatalytic properties of titanium dioxide (TiO_2). Chem Mater. 1993;5:280–3.
5. Zhang Z, Wang C, Zakaria R, Ying J. Role of particle size in nanocrystalline TiO_2-based photocatalysts. J Phys Chem B. 1998;102:10871–8.
6. Khan MA, Jung HT, Yang OB. Synthesis and characterization of ultrahigh crystalline TiO_2 nanotubes. J Phys Chem B. 2006;110: 6626–30.
7. Sun Y, Li A, Qi M, Zhang L, Yao X. High surface area anatase titania nanoparticles prepared by MOCVD. Mater Sci Eng B. 2001;86:185–8.
8. Xia B, Huang H, Xie Y. Heat treatment on TiO_2 nanoparticles prepared by vapor-phase hydrolysis. Mater Sci Eng B. 1999;57: 150–4.
9. Oskam G, Nellure A, Penn RL, Searson PC. The growth kinetics of TiO_2 nanoparticles from titania(IV) alkoxide at high water/ titanium ratio. J Phys Chem B. 2003;107:1734–8.
10. He D, Lin F. Preparation and photocatalytic activity of anatase TiO_2 nanocrystallites with high thermal stability. Mater Lett. 2007;61:3385–7.
11. Kormann C, Bahnemann DW, Hoffmann MR. Preparation and characterization of quantum size TiO_2. J Phys Chem. 1988;92: 5196–201.
12. Yanagisawa K, Ovenstone J. Crystallization of anatase from amorphous titania using the hydrothermal technique: effects of starting material and temperature. J Phys Chem B. 1999;103: 7781–7.
13. Hu Y, Tsai HL, Huang CL. Phase transformation of precipitated TiO_2 nanoparticles. Mater Sci Eng A. 2003;344:209–14.
14. Shen Q, Sato T, Hashimoto M, Chen C, Toyoda T. Photoacoustic and photo electrochemical characterization of CdSe-sensitized TiO_2 electrodes composed of nanotubes and nanowires. Thin Solid Films. 2006;499:299–305.
15. Robel I, Subramanian V, Kuno M, Kamat PV. Quantum dot solar cells. Harvesting light energy with CdSe nanocrystals molecularly linked to mesoscopic TiO_2 films. J Am Chem Soc. 2006; 128:2385–93.
16. Bang JH, Kamat PV. Quantum dot sensitized solar cells. A tale of two semiconductor nanocrystals: CdSe and CdTe. ACS Nano. 2009;3:1467–76.
17. Kongkanand A, Tvrdy K, Takechi K, Kuno K, Kamat PV. Quantum dot solar cells. Tuning photoresponse through size and shape control of CdSe–TiO_2 architecture. J Am Chem Soc. 2008;130(12):4007–15.
18. Natan MJ, Thackeray JW, Wrighton MS. Interaction of thiols with n-type cadmium sulfide and n-type cadmium selenide in aqueous solutions: adsorption of thiolate anion and efficient photoelectrochemical oxidation to disulfides. J Phys Chem B. 1986;90(17):4089–98.
19. Granot E, Patolsky F, Willner I. Electrochemical assembly of a CdS semiconductor nanoparticle monolayer on surfaces: structural properties and photoelectrochemical applications. J Phys Chem B. 2004;108(19):5875–81.
20. Lawless D, Kapoor S, Meisel D. Bifunctional capping of CdS nanoparticles and bridging to TiO_2. J Phys Chem. 1995;99(25): 10329–35.
21. Mann JR, Watson DF. Adsorption of CdSe nanoparticles to thiolated TiO_2 surfaces: influence of intralayer disulfide formation on CdSe surface coverage. Langmuir. 2007;23(22):10924–8.
22. Subramanian V, Wolf EE, Kamat PV. Catalysis with TiO_2/Au nanocomposites. Effect of metal particle size on the fermi level equilibration. J Am Chem Soc. 2004;126:4943–50.
23. Murray CB, Norris DJ, Bawendi MG. Synthesis and characterization of nearly monodisperse CdE (E = sulphur, selenium, tellurium) semiconductor nanocrystallites. J Am Chem Soc. 1993;115:8706–15.
24. Cullity BD. Elements of X-rays diffraction. Reading: Addison Wesley; 1978.
25. Tong T, Zhang J, Tian B, Chen F, He D. Preparation and characterization of anatase TiO_2 microspheres with porous frameworks via controlled hydrolysis of titanium alkoxide followed by hydrothermal treatment. Mater Lett. 2008;62:2970–2.
26. Deacon GB, Green JHS. Vibrational spectra of ligands and complexes. II. Infra-red spectra (3650–375 cm^{-1} of triphenylphosphine, triphenylphosphine oxide, and their complexes. Spectrochim Acta. 1968;24a:845–52.
27. Becerra LR, Murray CB, Griffin RG, Bawendi MG. Investigation of the surface morphology of capped CdSe nanocrystallites by ^{31}P nuclear magnetic resonance. J Chem Phys. 1994;100: 3297–300.
28. Dibbell RS, Soja GR, Hoth RM, Watson DF. Photocatalytic patterning of monolayers for the site-selective deposition of quantum dots onto TiO_2 surfaces. Langmuir. 2007;23:3432–9.
29. Deorsola FA, Valluari D. Synthesis of TiO_2 nanoparticles through gel combustion process. J Mater Sci. 2008;43:3274–8.
30. Marinescu C, Safronia A, Rusti C, Piticescu R, Badilita V, Vasile E, Baies R, Tanasescu S. DSC investigation of nanocrystalline TiO_2 powder. J Therm Anal Calorim. 2011;103:49–57.
31. Tauc J. In: Tauc J, editor. Amorphous and liquid semiconductors. New York: Plenum; 1974. p. 175.
32. Venkatachalam N, Palanichamy M, Murugesan V. Sol–gel preparation and characterization of alkaline earth metal doped nano TiO_2: efficient photocatalytic degradation of 4-chlorophenol. J Mol Catal A. 2007;273:177–85.
33. Wang H, Lewis JP. Second generation photocatalytic materials: anion doped TiO_2. J Phys Condens Matter. 2006;18:421.
34. Kavan L, Graitzel M, Gilbert SE, Klemenz C, Scheel HJ. Electrochemical and photoelectrochemical investigation of single-crystal anatase. J Am Chem Soc. 1996;118(28):6716–23.
35. Asahi R, Taga Y, Mannstadt W, Freeman AJ. Electronic and optical properties of anatase TiO_2. Phys Rev B. 2000;61:7459–65.
36. Serpone N, Lawless D, Khairutdinovt R. Size effects on the photophysical properties of colloidal anatase TiO_2 particles: Size quantization versus direct transitions in this indirect semiconductor? J Phys Chem. 1995;99:16646–54.
37. Jhonson SR, Tidies T. Temperature dependence of the Urbach edge in GsAs. J Appl Phys. 1995;78:5609–11.
38. Urbach F. The long-wavelength edge of photographic sensitivity and of the electronic absorption of solids. Phys Rev. 1953;92:1324.